INSTITUT DE FRANCE
Académie des sciences

Comptes Rendus

Chimie

Mabrouk Ben Hamden and Jamel Bouaziz

Preparation and characterization of tubular cermet membrane for microfiltration separation: application to the treatment of textile wastewater

Volume 24, issue 1 (2021), p. 135-146

Published online: 23 April 2021

https://doi.org/10.5802/crchim.69

Les Comptes Rendus. Chimie *sont membres du*
Centre Mersenne pour l'édition scientifique ouverte
www.centre-mersenne.org
e-ISSN : 1878-1543

Comptes Rendus
Chimie
2021, 24, nº 1, p. 135-146
https://doi.org/10.5802/crchim.69

Essay / *Essai*

Preparation and characterization of tubular cermet membrane for microfiltration separation: application to the treatment of textile wastewater

Mabrouk Ben Hamden[*, a] **and Jamel Bouaziz**[a]

[a] LAMA: Laboratory of Advanced Materials, National Engineering School, University of Sfax, BP 1173, 3038 Sfax, Tunisia

E-mails: benhamdenemabrouk@gmail.com (M. Ben Hamden), jamel.bouaziz@gmail.com (J. Bouaziz)

Abstract. Low-cost ceramic–metal composite (cermet) membrane supports have been elaborated and characterized. A plastic paste was prepared from kaolin (K), feldspar (F), sand (S), and two types of aluminum (i.e., waste aluminum alloy (WA) and commercial aluminum (CA)) mixed with water. This was followed by the preparation of a ceramic porous tube by extrusion and sintering at a temperature of 1350 °C for 2 h. The samples were then characterized using porosity, permeability, scanning electron microscopy (SEM), and chemical and mechanical properties to evaluate the effects of the addition of aluminum to the porcelain matrix on the mixture (50% K, 25% F, and 25% S). The microfiltration active layer was added on the support by a slip casting method using 63 μm kaolin powder, water, and polyvinyl alcohol solution (PVA); after drying at room temperature for 24 h, the microfiltration layer was heated to 650 °C for consolidation. SEM observation showed homogeneous layers without cracks with 5 μm and 9 μm thick layers for the two membranes prepared. Application of the membrane for the treatment of textile wastewater showed a turbidity removal of more than 98% and a chemical oxygen demand of more than 85%. This was a much better separation performance when compared to other membranes.

Keywords. Cermet, Waste aluminum alloy, Extrusion, Microfiltration membrane, Textile wastewater.

Manuscript received 19th October 2020, revised 24th December 2020 and 10th January 2021, accepted 2nd February 2021.

1. Introduction

The environment is a victim of several aggressive industrial activities. On the one hand, textile industries release huge amounts of wastewater causing serious damage to surface and underground water resources. As a rough estimation in sequence, to process a ton of textile, 230–270 tons of water has to be used [1–3]. The resulting effluents of such processes are highly loaded with organic pollutants such as salts and synthetic dyes [4]. In Tunisia, most of the textile industries discharge untreated wastewater into water bodies, which percolates into the groundwater, posing a threat to the health and socioeconomic life of the people. Pretreatment, dyeing, printing, and finishing

* Corresponding author.

Table 1. Chemical composition (mass %) of raw materials

Oxides	SiO_2	Al_2O_3	K_2O	Fe_2O_3	Na_2O	CaO	L.O.I*
K	48.47	36.43	0.97	0.88	0.63	—	12.07
F	79	12.45	2.8	—	4.58	0.47	0.6
S	94.58	0.93	0.29	—	3.81	—	0.36

L.O.I*: loss on ignition at 1000 °C.

are the main steps in the dyeing and printing process of textile industries [5]. A large amount of wastewater containing many pollutants like reactive dyes, chemicals, and organic compounds is being generated by all these processes.

On the other hand, large amounts of aluminum wastes are being rejected from industries every day in the form of chips and discards. The United States of America alone were reported to have released 20,000 metric tons of this scrap in 2017 [6]. Still worse, the chips deriving from the machining of semifinished aluminum products are very difficult to recycle by conventional methods due to their elongated spiral shape, small size, surface contamination with oxides, machining oil, etc. [7–10]. For this reason, Gronostajski *et al.* [8] reported that several techniques such as direct conversion of chips into compacted form, powder metallurgy, extrusion, and remelting by using protective salt were attempted to recycle these polluting materials. However, most of these efforts seemed to have achieved little success because of the high cost, complex techniques, and the absence of adequate technology. Therefore, aluminum scraps continue to be disposed of as solid waste and effluents from textile industries continue to contaminate the environment.

Therefore, the purpose of this study was to join the recent efforts of researchers such as Hamden *et al.* [11], Sayehi *et al.* [12], and Abid *et al.* [13] to valorize this environment pollutant by transforming it into a filtration membrane that can alleviate the dangers of the contaminating textile effluents. To reach this objective, this study purported to design a membrane made of ceramics and metal, called cermet, that would be capable of treating the contaminated effluents to a satisfactory level. The newly designed membrane would have many advantages. Besides ridding the environment of the poisonous dyes and heavy metals infecting the textile effluents, it would valorize the useless metallic scraps released by the various industries and reduce the cost of wastewater treatment since its basic raw materials such as the metallic particles, kaolin, feldspar, and sand would be either produced from industrial waste or freely available in the environment.

Table 2. Characteristics of the commercial aluminum powder used

Granulometry	100 μm–200 μm
Density (g/cm^3)	2.7
Purity	>99%

2. Materials and methods

2.1. *Materials and chemicals*

In this work, the raw materials used for the preparation of tubular supports and membranes were kaolin (K), feldspar (F), and sand (S) provided by CARTHAGO CERAMIC Ltd., Sfax, Tunisia. There are two types of aluminum: waste aluminum alloy (WA) in the form of new scrap collected from the metal manufacturing industry in the region of Sfax, Tunisia and commercial aluminum in the form of commercial powder (CA) acquired from Fluka. The chemical analysis that was determined by inductively coupled plasma (ICP) analysis is listed in Table 1.

Table 2 exhibits the main characteristics of the commercial aluminum powder used in this study. As can be clearly seen, its purity is greater than 99%.

Table 3 shows the chemical composition of the waste aluminum alloy (WA) revealed by the X-ray fluorescence (XRF) technique. As can be seen, this material contained 92.52% of aluminum. The rest was made of impurities of Ca, Ti, Si, Fe, and Mn derived from surface contamination with oxides and machining oil [9,10].

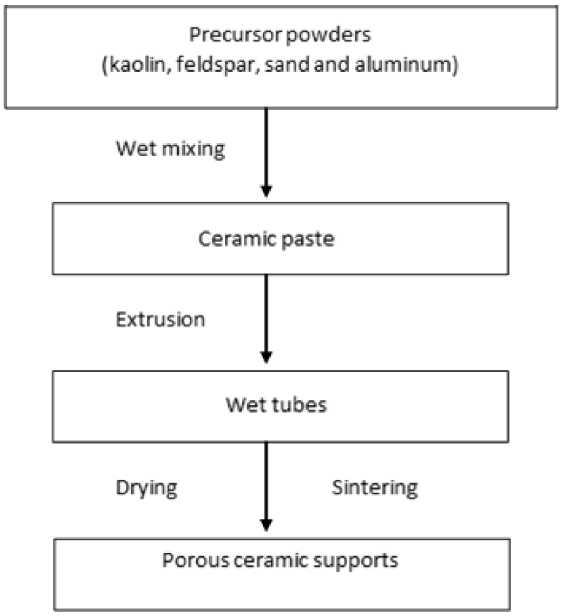

Figure 1. Main steps of the ceramic tubular support preparation.

Table 3. Chemical composition (mass %) of waste aluminum alloy

Compound	Al	Ca	Ti	Si	Fe	Mn
WA	92.52	1.58	2.49	1.71	0.79	0.46

2.2. *Elaboration of porous supports*

The preparation of tubular porous supports was achieved as follows:

- preparation of a plastic paste;
- shaping by extrusion;
- consolidation by sintering.

The procedure of the preparation of ceramic support is described in Figure 1. The powders were mixed using a rotary mixer at a speed of 65 rpm for 15 min, then kneaded by gradually adding distilled water and hydrochloric acid to adjust the pH to 4, to obtain a plastic paste with a good homogeneity and to allow the shaping. Thereafter, the paste was stored in a closed box for 48 h in a humid environment to improve its rheological property. After that, an extrusion technique was used to form some tubular samples. Tubular supports with external/internal diameter of 14/10 mm and length of 155 mm were produced. After extrusion, the wet supports were set on rollers to have a homogeneous drying at ambient temperature during 24 h. Finally, the extruded pieces were sintered using a programmable furnace (Nabertherm, Germany) according to the thermal cycle given in Figure 2. Two stages were determined: the first for the elimination of organic additives at 400 °C for 2 h and the second for the sintering at 1350 °C for 2 h. The photograph of the fabricated membrane supports is shown in Figure 3.

2.3. *Preparation of the kaolin microfiltration layer*

The active microfiltration layer from kaolin was prepared by a slip casting process. The optimal composition of the deflocculated slip was:

- 4 wt% of kaolin powder (100 g of natural kaolin was grinded using a planetary ball mill Retsch PM 100 at 400 rpm during 30 min, then calibrated with 63 μm);
- 40 wt% of polyvinyl alcohol (12 wt% aqueous solution);
- 56 wt% of water.

In the first step, a stable suspension has to be obtained by putting in suspension the kaolin powder in water. Then, 12 wt% aqueous solution of PVA was mixed to the preceding suspension. Deagglomeration of the mineral powder and homogenization of the coating formulation was ensured by mechanical stirring using an ordinary magnetic stirrer at its maximum speed. The coating formulation was poured inside the support for 6 min at room temperature while the tube was closed at one end. A layer was then formed on the inner side of the porous tube. Afterward, the excess was drained out. Drying was realized at room temperature for 24 h. The sintering temperature was fixed at 650 °C for 3 h. A heating temperature at 250 °C for 2 h is necessary in order to completely eliminate the PVA present in great quantity in the slip [14]. A relatively slow heating rate (2 °C/min) was needed in order to avoid the formation of cracks during the consolidation of the active layer.

2.4. *Characterization techniques*

In this study, different techniques were used to investigate the properties of the raw materials and the

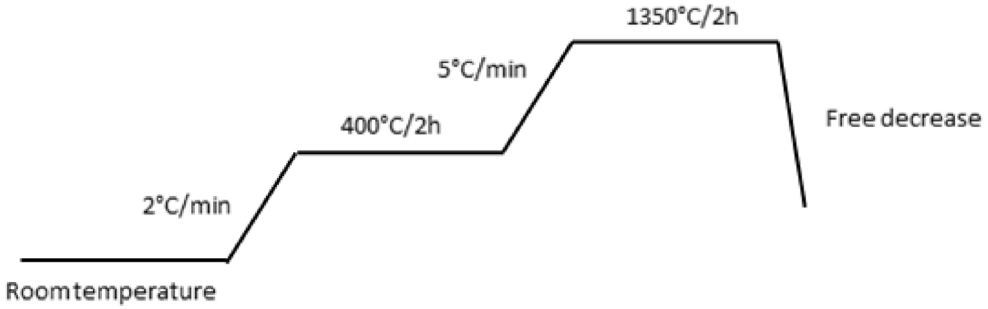

Figure 2. The thermal cycle used in the ceramic support sintering.

Figure 3. Photograph of porous tubular supports: support containing 0 wt% Al (a), support containing 4 wt% of WA (b), and support containing 4 wt% of CA (c).

ceramic membrane; namely, the particle size distribution, the X-ray diffraction (XRD), the mechanical strength, the chemical resistance, the total porosity, the mercury intrusion porosimetry, the water permeability, and the scanning electron microscopy (SEM).

Particle size distribution was measured using the laser particle size analysis (MASTERSIZER 2000). The test was conducted in water suspension. In order to avoid flocculation, samples were ultrasonicated for 5 min.

Phase identification was performed by XRD (D8 Bruker Advance) powder diffractometer using Kα1 radiation of Cu (λ = 0.15406 nm). XDR experiments were achieved in step-scan mode from 0° to 60° (2θ). The crystalline phases were identified using the computer program X′-pert High Score.

SEM was used to examine the morphology, surface quality, and thickness of intermediate top-layer membranes. The microstructure was analyzed using the Phillips XL 30 SEM working with 15 kV accelerating voltage.

The mechanical strength of sintered tubular supports was performed by the three-point bending method using a LLOYD EZ50 testing machine. The bending strength σ_f was calculated in the function of the following equation (Equation (1)) [15,16]:

$$\sigma_f = \frac{8 \cdot F \cdot L \cdot D_0}{\pi(D_0^4 - D_i^4)}, \quad (1)$$

where F is the measured force at which fracture takes place; L, D_0, and D_i are the length, external diameter, and internal diameter, respectively. In this study, the external diameter length of the tubular support was 95 mm, its external diameter was 14 mm, and its internal diameter was 10 mm.

The corrosion tests were conducted using aqueous solutions of nitric acid (0.45 M) and sodium hydroxide (0.5 M) at room temperature for 8 days. All

Table 4. Compositions and sample designations of the supports

Sample label	K (wt%)	F (wt%)	S (wt%)	WA (wt%)	CA (wt%)
T-M100	50	25	25	0	0
T-M96-WA4	48	24	24	4	0
T-M96-CA4	48	24	24	0	4
T-M90-WA10	45	22.5	22.5	10	0
T-M90-CA10	45	22.5	22.5	0	10

the samples were rinsed in distilled water and dried at 110 °C. The degree of corrosion was evaluated by the percentage of the weight loss.

The porosity of the sintered composites was determined by helium pycnometer (Micrometrics, Accupys//1340 Gas pycnometer). Four specimens were selected to determine porosity with an error of less than 1% of the measured porosity value.

The pore size distribution of the sintered ceramic supports was determined by a mercury intrusion porosimetry method (Micromeritics, Model Auto pore 9500).

The turbidity was measured using a Turbidimeter HACH RATIO 2100 A.

The laboratory pilot used for the filtration experiments was equipped with a cross-flow filtration system implementing a 15-cm long tubular ceramic membrane (Figure 4). The tubular membrane was placed in a stainless steel carter. The transmembrane pressure (TMP) ranging from 1 to 4 bars was ensured by an adjustable valve on the retentate side. Temperature was kept at 25 °C by a thermal exchange system. Before the filtration tests, the membrane underwent a preprocessing step by immersing it in distilled water for 24 h in order to get a constant flow at the beginning of each test [17].

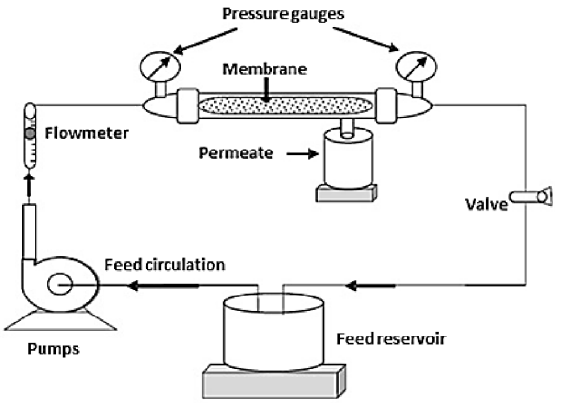

Figure 4. A schematic process used for the filtration system.

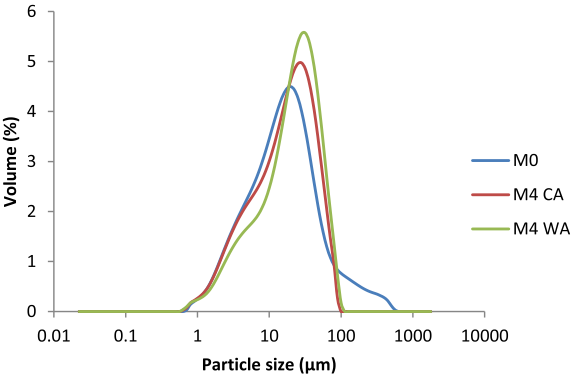

Figure 5. Particle size distributions of the mixtures containing 0 wt% of aluminum, 4 wt% of CA, and 4 wt% of WA.

2.5. *Compositions*

Table 4 summarizes the composition of the various samples.

3. Results and discussion

3.1. *Powder characterization*

In this study, both the supports and membranes were prepared from kaolin, feldspar, sand, and two types of aluminum. The raw materials used were characterized by Hamden *et al.* [11].

Figure 5 shows the evolution of the average particle size of the mixtures used to elaborate the supports. The curve revealed that the mixture prepared from kaolin, feldspar, and sand displayed a bimodal

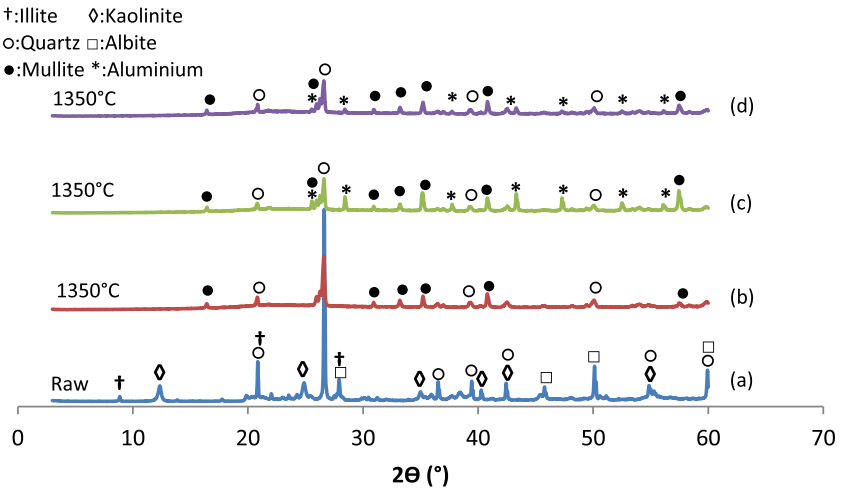

Figure 6. XRD diffractograms of the mixtures before and after heat treatment (T-M100 (a), T-M100 (b), T-M96-CA 4 (c), T-M96-WA 4 (d)).

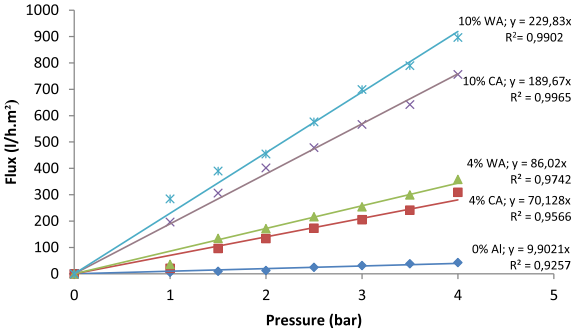

Figure 7. Water permeability of the tubular supports containing various weight percentages of aluminum after sintering at 1350 °C for 2 h.

particle size distribution with an average diameter (D50) of about 20 µm.

The particle size distribution was multimodal with D50 of approximately 23 µm and 29 µm for mixtures containing 4% of CA and WA, respectively. Hence, the addition of aluminum seemed to have caused a broader particle size distribution.

3.2. *Characterization of the support*

3.2.1. *Phase identification*

Figure 6 presents the XRD patterns of the raw and thermally treated composites. After heat treatment at 1350 °C for 2 h, all the peaks referring to kaolinite, illite, and albite disappeared and a new peak of mullite was detected. This mullite formation would be attributed to the reaction between metakaolin, feldspar, and sand. However, the peaks attributed to quartz remained unchanged, which would confirm the thermal stability of this phase during heat treatment.

3.2.2. *Determination of water permeability*

Figure 7 shows the results of the variation of water permeability for the prepared supports sintered at 1350 °C for 2 h. The flux showed a linear evolution in the function of the pressure and the percentage of aluminum. The water flux through the membranes follows Darcy's Law:

$$J_w = L_p \Delta P,$$

where L_p is the permeability of solvent (L/h·m^2·bar) and ΔP (bar) is the applied TMP. Hence, the hydraulic permeability showed approximately a ten-fold increase after the addition of 4 wt% of aluminum to the mixture. Indeed, the 4 wt% addition of WA boosted the permeability from 9.9 to 86 L·h^{-1}·m^{-2}·bar^{-1} at a pressure of 4 bar. Similarly, the 4 wt% addition of CA resulted in a permeability of 70.12 L·h^{-1}·m^{-2}·bar^{-1} at the same pressure. Then, the hydraulic permeability continued to rise steadily with the increase of aluminum percentage and the pressure to reach 229.83 and 189.67 L·h^{-1}·m^{-2}·bar^{-1} with the addition

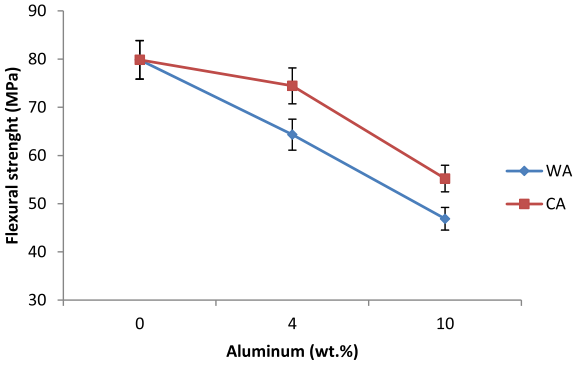

Figure 8. Flexural strength of the tubular supports with different wt% of aluminum sintered at 1350 °C for 2 h.

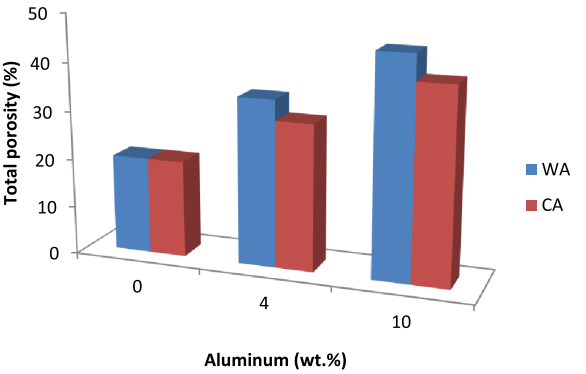

Figure 9. Total porosity of the tubular supports with different wt% of aluminum sintered at 1350 °C for 2 h.

of 10 wt% of WA and CA, respectively. As was demonstrated by Issaoui *et al.* [18] in an earlier work, an increase of metal contents to the porcelain supports causes a higher flux. This was rightly explained by the exothermic oxidation reaction of aluminum which produces H_2 gas and germination of the α-alumina phase that reacts with the metal-kaolin to produce porous mullite. Issaoui *et al.* [19] confirmed this idea and added that such a reaction creates bigger voids and pores in the elaborated cermet supports.

3.2.3. *Mechanical strength*

The mechanical resistance test was performed using the three points bending strength to control the resistance of the support elaborated with different wt% aluminum and sintered at 1350 °C for 2 h. The bending strength of the support samples is shown in Figure 8. There was a slight decrease in the bending strength as a function of the increase of the metal amounts from 0 to 10 wt%. This would be explained by the increase of H_2 gas formation creating voids from the dissolution of aluminum in water-based suspensions, which would promote the fragility of the ceramic supports.

3.2.4. *Total porosity*

Figure 9 shows the total porosity of tubular supports with different wt% of WA and CA, sintered at 1350 °C for 2 h. As can be seen from the bar diagram, the addition of aluminum to the mixture increased the porosity of the membrane. Furthermore, the addition of WA resulted in the creation of a higher porosity than that of CA independently of the added amount. Finally, the addition of 10 wt% yielded the highest porosity for both samples. Indeed, total porosity increased from 20 to 45% as the added amount of aluminum rose from 0 to 10 wt%. In line with Issaoui *et al.* [18], this study would explain this phenomenon by the fact that the exothermic oxidation reaction of aluminum leaves behind voids which would become pores.

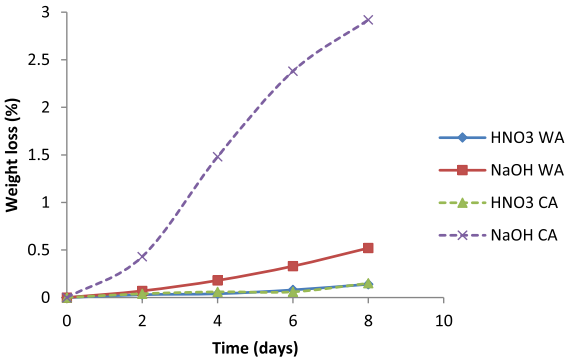

Figure 10. Weight loss of supports containing 4 wt% of WA and 4 wt% of CA sintered at 1350 °C for 2 h in HNO_3 and NaOH as a function of time.

3.2.5. *Chemical resistance*

The supports sintered at 1350 °C for 2 h were subjected to corrosion resistance tests. The supports were soaked at room temperature in solutions of NaOH and of HNO_3. The control of weight loss was for 8 days. Figure 10 exhibits the weight loss of

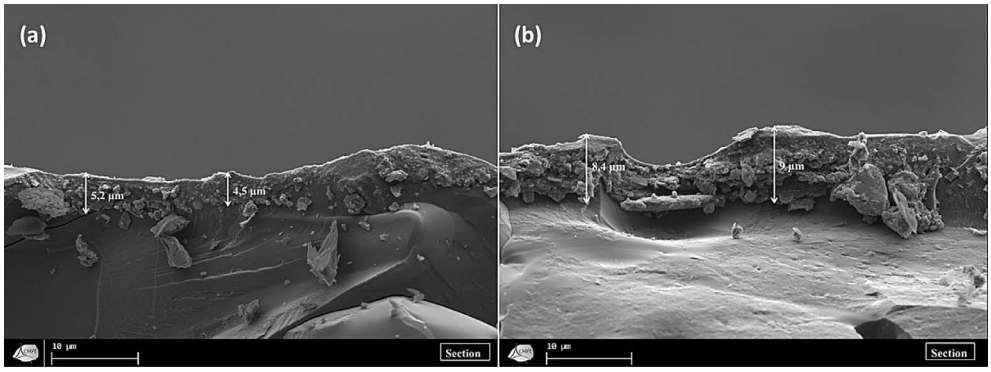

Figure 11. SEM micrographs of the cross-section of the microfiltration containing 4 wt% of WA (a) and the microfiltration membrane containing 4 wt% of CA (b) sintered at 650 °C.

supports containing 4 wt% of WA and 4% of CA sintered at 1350 °C for 2 h in NaOH and HNO_3 as a function of time. The degree of corrosion was characterized by the percentage of the mass loss. The membrane supports showed a better acid corrosion resistance than alkali. This could be due to the fact that the reaction of the glass phase in the samples with HNO_3 solution was more difficult to occur than with NaOH solution. Actually, it was the SiO_2 in the glass phase that hardly reacted with HNO_3. In line with Gao *et al.* [20], the Gibbs free energy between Al_2O_3 and H^+ obtained from the Microsoft "HSC Chemistry 6" was equal to -112 KJ·mol^{-1} while that of Al_2O_3 and OH^- was equal to -10.56 KJ·mol^{-1}. However, the SiO_2 value contained in the glass phase was higher than the Al_2O_3 value, due to the relatively low dissolution and diffusion rates of the coarse alumina. In other words, the reaction between SiO_2 and OH^- represented by Gibbs free energy, which was equal to -1075 KJ·mol^{-1}, was dominant. Therefore, the mass loss was lower in HNO_3 than that in NaOH.

Therefore, the observed results in mass loss during corrosion tests suggest that the prepared supports had a good chemical corrosion resistance and were suitable for applications involving acidic and basic media.

3.3. *Characterization of the microfiltration layer*

3.3.1. *Scanning electron microscopy*

Figure 11 exhibits two SEM micrographs of the section of the microfiltration membranes sintered at 650 °C containing 4 wt% of WA and CA, respectively. Firstly, it was observed that the thickness of the filtration layer was about 5 and 8.5 µm for the membrane containing WA and that containing CA, respectively. Secondly, the membrane surfaces seemed very homogeneous and showed no cracks. Thirdly, there seemed to be a strong adhesion between the support and the microlayer. Therefore, it can be concluded that the homogeneity of the membrane surface, the strong adhesion between the layers, and their thickness can be considered very adequate characteristics of an efficient filtration membrane.

3.3.2. *Mercury porosimetry*

The average pore size of the optimized membranes containing 4 wt% of WA and those containing 4 wt% of CA was determined by mercury porosimetry. The pore diameter was centered around 0.8 µm for the former and 1 µm for the latter (Figures 12 and 13), which would confirm that a microfiltration layer was achieved.

3.3.3. *Determination of microfiltration membrane permeability*

Figure 14 shows the water flux permeability in function of the working pressure of the support and the membrane containing 4 wt% of WA and that containing 4 wt% of CA, both sintered at 1350 °C for 2 h. Firstly, the water permeability of the membranes was of 21.4 l/h·m^2·bar for the membrane with WA and 22.73 L/h·m^2·bar for that with CA. Secondly, it was clearly observed that the increase of the applied pressure resulted in a linear increase of the water flux through both membranes. Finally, the flux of water

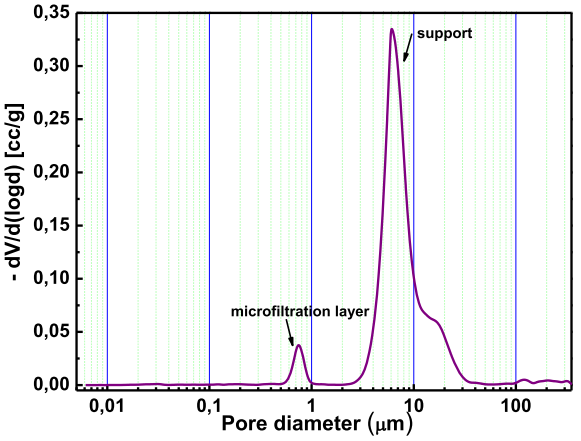

Figure 12. Pore size distribution of the membrane containing 4 wt% of WA sintered at 650 °C.

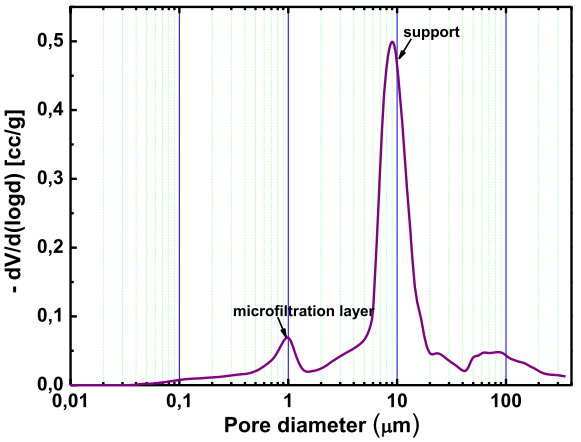

Figure 13. Pore size distribution of the membrane containing 4 wt% of CA sintered at 650 °C.

followed the same pattern for the support and the membrane despite the big difference in their permeability rates.

3.4. *Application to the treatment of the textile effluents: permeation properties and removal efficiency*

The study was conducted with real effluent textile industry wastewater collected from the sewage of a textile factory in the area of Ksar Hellal, Tunisia. As was characterized by Masmoudi *et al.* [21], textile

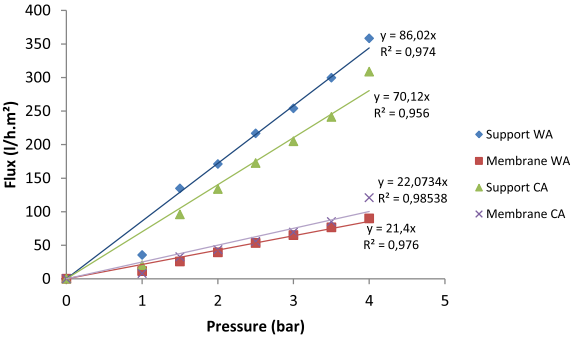

Figure 14. Water flux permeability versus working pressure of supports and membranes containing 4 wt% of WA and 4 wt% of CA sintered at 1350 °C for 2 h.

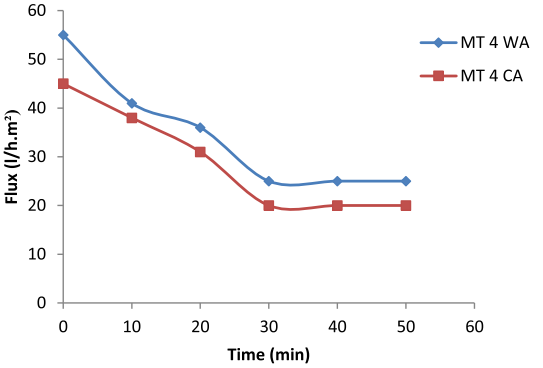

Figure 15. Variation of permeate flux in function of time (T = 25 °C, TMP = 4 bar).

wastewaters usually consisted of various pollutants emanating from the dyeing, washing, and bleaching baths and particularly contained chemical substances such as hydrolyzed reactive dyes, detergents, salts, and auxiliaries such as surfactants and emulsifiers. The initial physicochemical characteristics of the raw effluents are given in Table 5 in terms of conductivity, chemical oxygen demand (COD), turbidity, and salinity.

Cross-flow filtration tests of wastewater were performed on two composite membranes containing 4 wt% of WA and 4 wt% of CA, respectively.

In this study, permeate flux of feed samples was performed in function on working time through the two CA and WA membranes as provided in Figure 15. Rapid and linear membrane flux declines were observed during the first 30 min for both CA

Table 5. Characteristics of the effluent before and after filtration

	Conductivity ($mS{\cdot}cm^{-1}$)	COD ($mg{\cdot}L^{-1}$)	Turbidity (NTU)	Salinity ($g{\cdot}L^{-1}$)
Raw effluent	2.94	795	135	1.59
Permeate MT-4 CA	2.81	98	1.5	1.52
Permeate MT-4 WA	2.86	110	2.1	1.53

and WA membranes. Then flux stabilized and permeate flux values of 20 $L{\cdot}m^{-2}{\cdot}h^{-1}$ and 25 $L{\cdot}m^{-2}{\cdot}h^{-1}$ corresponding to AW and AC membranes were recorded, respectively.

The flux decline behavior can be explained by the faster formation of cake by the suspended particulates and the organic substances retained on the membrane surface, which allows the mass transfer limitation. In line with Jung [22] and Han *et al.* [23], this behavior can be explained by the formation of concentration polarization and fouling due to the interaction between the membrane material and the solution.

Membranes developed here could be used to treat textile effluents in order to reuse water and/or to recover valuable species. In this context, reducing pollution and discoloring feed solutions by using developed WA and CA membranes were studied. Permeate samples were taken at the end of each filtration experiment and analyzed to determine the removal efficiency in terms of conductivity, COD, turbidity, and salinity.

Table 5 exhibits the characteristics of the effluent before and after filtration. It was clearly observed that using the colorimetric method, the microfiltration through the membranes of CA and WA proved to be very efficient in reducing the COD. Indeed, the content in COD dropped from 795 to 98 $mg{\cdot}L^{-1}$ and to 110 $mg{\cdot}L^{-1}$, respectively. Equally, both membranes showed a satisfactory efficiency in decreasing the turbidity of the effluent. The water turbidity was reduced from 135 NTU to 1.5 and 2.1 NTU, respectively. However, the conductivity and the salinity were not.

Here, the MF membrane exhibits a high rejection of COD, turbidity, and color removal efficiency (%) demonstrating the high performances of both these novel membranes toward industrial wastewater treatment. The high rejection performances by the microfiltration are surprising given the membrane pore size.

Although comprehensive discussion of the mechanism of dye removal requires further investigation, it may be assumed that the efficiency of the MF process results from a delicate balance of filtration process and interaction between the membrane surface and the dye molecules.

It is to highlight that, Oun *et al.* [24] have explained the complete elimination of the alizarin red dye to the potential interactions between membrane materials and dye solutions.

Additionally, it is well known that these aromatic molecules tend to aggregate due to hydrophobic interactions between the aromatic rings of adjacent molecules during the filtration process [25].

The improved rejection of the molecules rejection may be due to the hydrogen bond and the formation of molecule clusters; then, electrostatic repulsion effect can be enhanced and contributes to the rejection of high pollutant molecules. Consequently, the high rejection of these organic pollutants is due to the synergistic effects of the increase in molecule size through aggregation and the strong electrostatic exclusion effect from the membrane surface.

On the other hand, the adsorption of molecules onto membrane surface during filtration can allow the enhancement of the concentration polarization layer and then result in more retention and thus the increasing of rejection efficiency [26,27]. This was also consistent with the observed decline in permeate flux (Figure 15). Finally, given that microfiltration range (0.1 μm–10 μm) remains inefficient for rejection of salts, no remarkable decrease of salinity and conductivity was recorded, as can be seen from Table 5.

3.5. *Membrane regeneration*

At the implementation of the microfiltration membrane, there was an observed limitation caused by the inevitable phenomenon of irreversible fouling.

Table 6. Acido-basic washing sequence

Sequence	Agent	Concentration	T (°C)	Pressure (bar)	Time (min)
Rinsing then evacuation	Water		RT	3	
Basic washing	NaOH	5–10 g·L^{-1}	60–70	3	30
Rinsing until neutrality	Water		RT	3	
Acidic washing	HNO_3	5 ml·L^{-1}	40–50	3	30
Rinsing until neutrality			RT	3	

*RT: room temperature.

Indeed, this caused the permeate flux to decline and then represented a serious obstacle for the performance of the membrane. This was explained by Han *et al.* [28] by the hydrophilic–hydrophobic interactions between membrane surfaces and the permeate. In this study, the hydrophobic membrane fouling observed during the treatment process would be attributed to the absence of hydrogen bonding interactions at the membrane interface level. Table 6 shows the acido-basic and distilled water regeneration sequence.

The regeneration accomplishment of the membrane would be determined by its recuperation of a permeability equal to that before clogging. Figure 16 shows the variation of the permeate flux through both membranes WA and CA before and after regeneration.

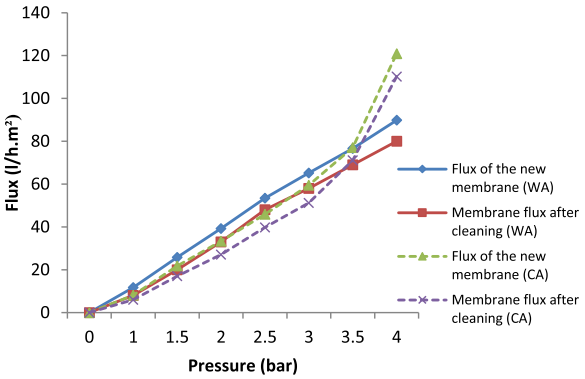

Figure 16. Variation of the permeate flux before and after regeneration of membranes with 4 wt% of WA and 4 wt% of CA.

3.6. *Comparative study*

Industrially, it is important to analyze the cost of any process to determine its practical feasibility. Extensive research was carried out to develop low-cost ceramic membranes with high performance for different environmental applications, such as the treatment of industry wastewaters [29–31], oily wastes [32], and textile sludge [33]. In fact, the use of ceramic membranes in the field of wastewater treatment is still limited because of their higher cost [34], as it is approximately 10 times higher than that of polymer membranes [35]. Hence, a low-cost material for the fabrication of ceramic membrane is needed. In this study, porous ceramic membranes for filtration were successfully fabricated via kaolin and aluminum powders. In terms of price, the cost of membrane containing CA is higher than the membrane prepared by the waste aluminum alloy (WA) since 1 kg of CA is purchased from Fluka (Spain) at €250 while WA is provided at no cost from local companies which dispose it as a waste. It can be said that the membrane containing waste aluminum alloy is economical, environment friendly, and does not need any further processing before using it, making it a better choice as an additive to ceramics for the fabrication of cermet membranes to be implemented in textile wastewater treatment.

4. Conclusion

This study presented the elaboration and implementation of two membranes made of ceramics and CA or WA intended for the filtration of textile wastewater. The membranes were prepared by the extrusion procedure. It revealed that the addition of the metal would increase the porosity of the membranes. The active microfiltration layer obtained by slip casting

process showed a satisfactory adhesion to the support. Furthermore, the application of the microfiltration membranes to the treatment of textile effluents yielded very satisfactory results in terms of COD and turbidity reduction and color improvement of the treated effluent. Finally, the work compared the performance of the membranes with CA with that with WA. The tests revealed a slightly better performance of the former. However, because of the availability of WA at a lower cost than CA, and its environment polluting character, it would be much more beneficial to use it as an additive to kaolin instead of CA. In addition to the economic and environmental advantages of the WA membranes, they may be used as a support for ultrafiltration.

Acknowledgments

The Ministry of Higher Education and Scientific Research of Tunisia supported this study financially. Moreover, the authors would like to thank Dr. Abdallah Oun for his helpful suggestions and technical support at UPEC and Sfax University. The authors also extend their gratitude to Dr. Ayadi Hajji for proofreading, correcting, and improving the English of the manuscript.

References

[1] J. Lin, W. Ye, H. Zeng, H. Yang, J. Shen, S. Darvishmanesh, P. Luis, A. Sotto, B. Van der Bruggen, *J. Membr. Sci.*, 2015, **477**, 183-193.

[2] J. Lin, W. Ye, J. Huang, B. Ricard, M. Baltaru, B. Greydanus, S. Balta, J. Shen, M. Vlad, A. Sotto, P. Luis, B. Van der Bruggen, *J. Chem. Eng.*, 2015, **3–9**, 1993-2001.

[3] J. Lin, C. Y. Tang, W. Ye, S. P. Sun, S. H. Hamdan, A. Volodin, C. V. Haesendonck, A. Sotto, P. Luis, B. Van der Bruggen, *J. Membr. Sci.*, 2015, **493**, 690-702.

[4] M. Vedrenne, R. Vasquez-Medranoa, D. Prato-Garciaa, B. A. Frontana-Uribec, M. Hernandez-Esparza, J. M. Andrés, *J. Hazard. Mater.*, 2012, **243**, 292-301.

[5] K. Siddique, M. Rizwan, M. J. Shahid, S. Ali, R. Ahmad, H. Rizvi, "Textile Wastewater Treatment Options: A Critical Review", in *Enhancing Cleanup of Environmental Pollutants* (N. Anjum, S. S. Gill, N. Tuteja, eds.), Springer, 2017, 183-207.

[6] National Minerals Information Center, "International Minerals Statistics and Information (USGS)", 2018, Available online at http://minerals.usgs.gov/minerals/pubs/country/.

[7] J. Gronostajski, A. Matuszak, *J. Mater. Process. Technol.*, 1999, **92–93**, 35-41.

[8] J. Gronostajski, H. Marciniak, A. Matuszak, *J. Mater. Process. Technol.*, 2000, **106**, 34-39.

[9] M. Samuel, *J. Mater. Process. Technol.*, 2003, **135**, 117-124.

[10] J. B. Fogagnolo, E. M. Ruiz-Navas, M. A. Simón, M. A. Martinez, *J. Mater. Process. Technol.*, 2003, **143–144**, 792-795.

[11] M. B. Hamden, G. Lecomte-Nana, J. Bouaziz, *J. Desalin. Water Treat.*, 2019, **147**, 73-82.

[12] M. Sayehi, H. Tounsi, G. Garbarino, P. Riani, G. Busca, *Waste Manag.*, 2020, **103**, 146-158.

[13] R. Abid, G. Delahay, H. Tounsi, *J. Mater. Cycles Waste Manag.*, 2019, **21**, 1188-1196.

[14] S. Masmoudi, R. B. Amar, A. Larbot, A. El Feki, A. B. Salah, *J. Membr. Sci.*, 2005, **247**, 1-9.

[15] J. N. Cernica, *Strenght of Materials*, 2nd ed., Holt, Rinchart & Winstron, New York, 1977.

[16] J. B. Wachtman, *Mechanical Properties of Ceramics*, Wiley, New York, 1996.

[17] J. M. Benito, M. J. Sánchez, P. Pena, M. A. Rodríguez, *J. Desalination*, 2007, **214**, 91-101.

[18] M. Issaoui, J. Bouaziz, M. Fourati, *J. Desalin. Water Treat.*, 2015, **53**, 1037-1044.

[19] M. Issaoui, L. Limousy, B. Lebeau, J. Bouaziz, M. Fourati, *C. R. Chim.*, 2016, **19**, 496-504.

[20] Z. F. Gao, B. Q. Wang, J. W. Yin, Y. P. Zeng, *Int. J. Appl. Ceram.*, 2019, **16**, 335-345.

[21] G. Masmoudi, E. Ellouze, F. El Ayni, R. Ben Amor, *J. Desalin. Water Treat.*, 2013, **52**, 2322-2329.

[22] B. Jung, *J. Membr. Sci.*, 2004, **229**, 129-136.

[23] B. Han, D. Zhang, Z. Shao, L. Kong, L. Shaoyi, *J. Desalin.*, 2013, **311**, 80-89.

[24] A. Oun, T. Nouha, S. Mahouche-Chergui, C. Carbonnier, S. Majumdar, S. Sarkar, G. C. Sahoo, R. Ben Amar, *Sep. Purif. Technol.*, 2017, **188**, 126-133.

[25] J. Lin, W. Ye, M. C. Baltaru, Y. P. Tang, N. J. Bernstein, P. Gao, S. Balta, M. Vlad, A. Volodin, A. Sotto, P. Luis, A. L. Zydney, B. Van der Bruggen, *J. Membr. Sci.*, 2016, **514**, 217-228.

[26] A. Karim, B. Achiou, A. Bouazizi, A. Aaddane, M. Ouammou, M. Bouziane, J. Bennazha, S. A. Younssi, *J. Environ. Chem. Eng.*, 2018, **6**, 1475-1485.

[27] A. Bouazizi, M. Breida, A. Karim, B. Achiou, M. Ouammou, J. I. Calvo, A. Aaddane, K. Khiat, S. A. Younssi, *Ceram Int.*, 2017, **43**, 1479-1487.

[28] W. Han, H. P. Gregor, E. M. Pearce, *J. Appl. Polym. Sci.*, 2000, **77**, 1600-1606.

[29] K. Ramesh, C. Sankha, P. Parimal, *Environ. Sci. Pollut. Res.*, 2015, **22**, 6010-6023.

[30] L. Jian, H. Zhen, *Environ. Sci. Pollut. Res.*, 2016, **23**, 3897-3906.

[31] V. Innocenzi, M. Prisciandaro, G. M. di Celso, F. Vegliò, *Waste Manag.*, 2018, **74**, 393-403.

[32] Y. Rasouli, M. Abbasi, S. A. Hashemifard, *J. Clean. Prod.*, 2017, **161**, 545-559.

[33] M. Wang, M. Mao, M. Zhang, G. Wen, Q. Yang, B. Su, *Q. Waste Manag.*, 2019, **91**, 29-36.

[34] S. Jana, M. K. Purkait, M. Kautubha, *Appl. Clay Sci.*, 2010, **47**, 317-324.

[35] R. V. Kumar, L. Goswami, K. Pakshirajan, G. Pugazhenthi, *J. Water Process. Eng.*, 2016, **13**, 168-175.